An Improved Coupled Model for ENSO Prediction and Implications for Ocean Initialization. Part I: The Ocean Data Assimilation System

David W. Behringer, Ming Ji, and Ants Leetmaa

National Centers for Environmental Prediction, NWS/NOAA, Washington, D.C.

(Manuscript received 1 October 1996, in final form 26 August 1997)

ABSTRACT

An improved forecast system has been developed for El Niño–Southern Oscillation (ENSO) prediction at the National Centers for Environmental Prediction. Improvements have been made both to the ocean data assimilation system and to the coupled ocean–atmosphere forecast model. In Part I of a two-part paper the authors describe the new assimilation system. The important changes are 1) the incorporation of vertical variation in the first-guess error variance that concentrates temperature corrections in the thermocline and 2) the overall reduction in the magnitude of the estimated first-guess error. The new system was used to produce a set of retrospective ocean analyses for 1980–95. The new analyses are less noisy than their earlier counterparts and compare more favorably with independent measurements of temperature, currents, and sea surface height variability. Part II of this work presents the results of using these analyses to initialize the coupled forecast model for ENSO prediction.

1. Introduction

For more than a decade, beginning with the early success of Cane et al. (1986), the application of coupled ocean–atmosphere models to the problem of making credible forecasts of the El Niño–Southern Oscillation (ENSO) phenomenon has been an area of active research (Latif et al. 1993; Ji et al. 1994; Chen et al. 1995; Rosati et al. 1997). In this two-part paper we describe recent improvements to the forecast system at the National Centers for Environmental Prediction (NCEP). Both the coupled model and the ocean analysis system used to initialize the forecast have been improved. The changes to the analysis system are modest, but the effect of those changes is significant, both in bringing the ocean analyses closer to independent measurements of the ocean and in improving the ENSO forecasts. Thus a brief description the new analysis system seems warranted and that is the objective of Part I. The improved ENSO forecasts are the subject of the longer Part II (Ji et al. 1998).

2. The ocean analysis system

A fundamental part of the ENSO forecast problem is the initialization of the ocean component of the coupled model. Zebiak and Cane (1987) accomplished this initialization by using a wind stress field derived from observed Pacific winds to drive the ocean model prior to the start of a forecast cycle. Others have subsequently used similar methods (Latif et al. 1993; Kleeman 1993; Chen et al. 1995; Kirtman et al. 1997). A different approach drives the ocean model with surface wind data but also attempts to correct the model temperature field by assimilating measurements of surface and subsurface temperature (Ji et al. 1994; Kleeman et al. 1995; Rosati et al. 1997). At NCEP we have followed the second approach combining an ocean general circulation model evolved from the model developed at Geophysical Fluid Dynamical Laboratory (Bryan 1969; Cox 1984; Philander et al. 1987) with the variational data assimilation method of Derber and Rosati (1989).

a. The model

The version of the ocean model that we currently use is the Modular Ocean Model (MOM), version 1, and we have configured it for the Pacific Ocean from 45°S to 55°N and 120°E to 70°W. The horizontal resolution in the zonal direction is 1.5°, while the resolution in the meridional direction is ⅓° within 10° of the equator, smoothly changing to 1° poleward of 20° latitude. There are 28 vertical levels with 18 concentrated in the top 400 m of the ocean. This has been our standard model for several years and further details of its configuration can be found in Ji et al. (1995).

The only model change that has been made for the new analysis system is in the choice of one of the parameters in the vertical mixing scheme. We use the Richardson number–dependent scheme of Pacanowski and

Corresponding author address: Dr. Ming Ji, Climate Modeling Branch, National Centers for Environmental Prediction, 5200 Auth Road, Rm. 807, Camp Springs, MD 20746.
E-mail: ming.ji@noaa.gov

Philander (1981), in which the coefficient for vertical eddy viscosity ν is given by

$$\nu = \frac{\nu_0}{(1 + \alpha R_i)^n} + \nu_b, \quad (1)$$

where R_i is the Richardson number and ν_b, ν_0, and n, are parameters to be chosen empirically. Pacanowski and Philander (1981) recommend values of $\nu_b = 1.0$ cm^2 s^{-1}, $\alpha = 5$, $n = 2$, and $\nu_0 = O(50$ cm^2 s$^{-1})$. Based on early experiments with the coupled forecast model we had set $\nu_0 = 5$ cm^2 s^{-1}. It has subsequently become clear that this value is too small, resulting in too little mixing of momentum down through the top of the thermocline and a core depth of the Equatorial Undercurrent that is too shallow. For the new analysis system we have turned back to the original recommendations and set $\nu_0 = 50$ cm^2 s^{-1}.

b. The assimilation system

The analysis system uses the three-dimensional variational scheme of Derber and Rosati (1989) to assimilate measurements of surface and subsurface temperature. The scheme computes an update or correction to the model temperature field by simultaneously minimizing the differences between the corrected temperature field and the current model solution and the corrected temperature field and the measured temperatures. Each of these differences is weighted by an appropriate error covariance function. The functional to be minimized is

$$\mathsf{I} = \frac{1}{2}\mathbf{T}^{\mathrm{T}}\mathbf{E}^{-1}\mathbf{T} + \frac{1}{2}[\mathbf{D}(\mathbf{T}) - \mathbf{T}_0]^{\mathrm{T}}\mathbf{F}^{-1}[\mathbf{D}(\mathbf{T}) - \mathbf{T}_0], \quad (2)$$

where the vector $\mathbf{T}$ represents the correction to the first-guess temperature field computed by the model, $\mathbf{E}$ is the first-guess error covariance matrix, the vector, $\mathbf{T}_0$ represents the difference between the temperature observations and the first-guess field, $\mathbf{D}$ is an interpolation operator from the model grid to the observation locations, and $\mathbf{F}$ is the observation error covariance matrix for temperature.

The estimated error covariance matrices, $\mathbf{E}$ and $\mathbf{F}$, determine the spatial structure and the magnitude of the temperature corrections. For the $\mathbf{E}$ matrix we have retained the original specification of Derber and Rosati (1989), so that the horizontal covariance between any two points is given by

$$a_h \exp\left(-\frac{r^2}{b^2 \cos\phi}\right), \quad (3)$$

where $a_h = 0.01$ and ϕ is the latitude. The parameter b, which was held constant at 4° in earlier analyses, has been modified, setting $b^2 = b_{\mathrm{lat}}^2 + b_{\mathrm{long}}^2$, to allow stretching of the horizontal covariance scale in the zonal direction. The parameter b_{lat} remains constant at 4°, while b_{long} is allowed to vary, providing relatively more stretching of the zonal scale toward the equator. Figure 1 illustrates the effect.

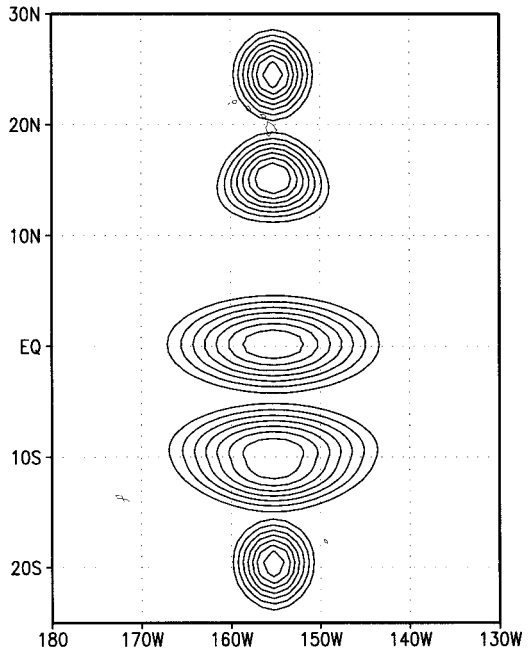

FIG. 1. Example of horizontal first-guess error covariance for unit observations at latitudes (from top to bottom) 25°N, 15°N, 0°, 10°S, and 20°S (note that the error covariance is symmetric about the equator).

In earlier analyses, the first-guess error variance a_h was held constant throughout the basin and at all depths. In those analyses, we found that the magnitude of the model–data differences and thus the magnitude of the temperature correction was largest in the thermocline. Furthermore, we found that the vertical profile of the variance of the temperature correction was proportional to the local profile of $(dT/dz)^{1/2}$. In the new analyses system we therefore scale the first-guess error variance by the factor

$$a_v \frac{(dT/dz)^{1/2}}{[(dT/dz)^{1/2}]_{b\max}}, \quad (4)$$

where the denominator is constant and represents a basin wide maximum value used to normalize the expression. The constant a_v is determined empirically by tuning the analysis; we have set $a_v = 1.3$. Figure 2 shows examples of the vertical structure of the error variance at several geographical locations for July 1992. In our study, the vertical structure of the error variance is estimated each month based on a set of previously produced analysis. Alternatively, in producing real-time analyses, these could be estimated from the analysis for the previous month or week.

For the observational error covariance matrix $\mathbf{F}$, we assume that the observations are uncorrelated. Therefore, $\mathbf{F}$ has only diagonal elements, which are the error variances for the data. In the new system, estimates of

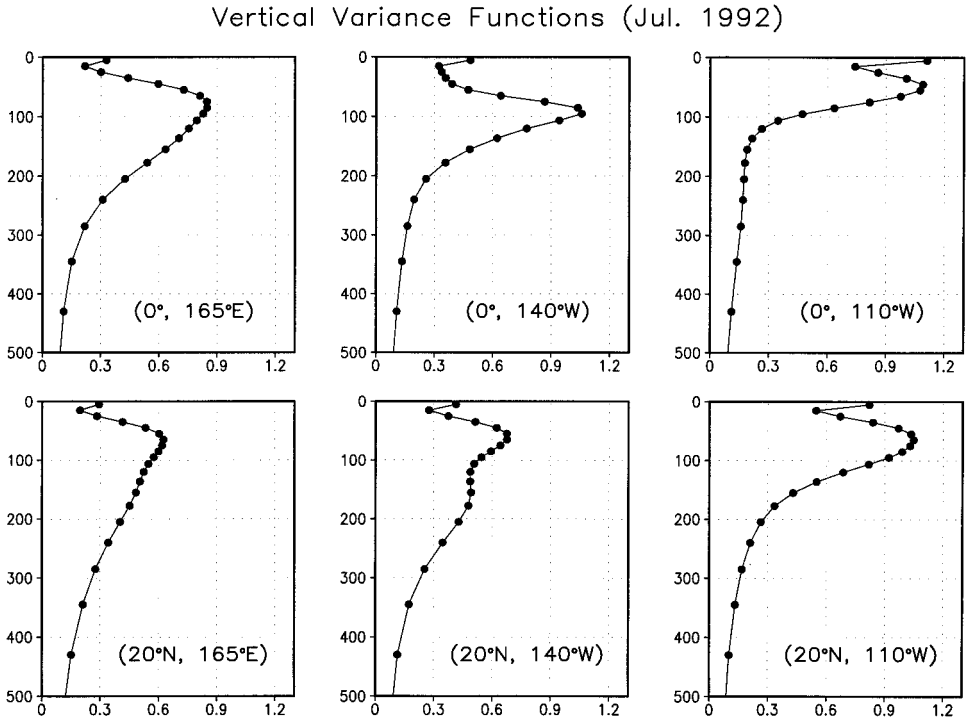

FIG. 2. Example of vertical first-guess error covariance for July 1992 at selected geographical locations in the tropical Pacific.

the observational errors assigned to subsurface temperatures from expendable bathythermographs (XBT) and from moored buoys are proportional to the local vertical temperature gradient dT/dz, which is computed directly from each individual temperature profile (J. Derber 1995, personal communication). This approach differs from the method used by Ji et al. (1995), who estimated dT/dz from a prescribed reference temperature field produced by the model. The resultant error estimates for both XBT and TAO (tropical atmosphere–ocean array) data are in the range of 1°–2.5°C, which are in the same range as those used by Ji et al. (1995).

The assimilation scheme uses all the data that fall within a specified time window centered on the current model time. For subsurface temperature data the window extends from -2 weeks to $+2$ weeks, while for the surface temperature the window runs from -1 week to $+1$ week. Data that is more distant from the current time is given less weight in the assimilation. How the matrix $\mathbf{F}$ is modified to accomplish this is discussed in Derber and Rosati (1989) as is the method for minimizing the functional (2).

3. The ocean analyses

Three sets of monthly analyses have been done for the Pacific, all approximately 15 years in length. Each analysis was forced by the climatological mean annual cycle of wind stress of Hellerman and Rosenstein (1983) combined with monthly anomalies derived from the pseudostress fields of Stricherz et al. (1992), which are also known as the Florida State University (FSU) wind analyses. The heat flux forcing was the climatological mean annual cycle of Oberhuber (1988); there was no freshwater flux forcing; instead, the model's surface salinity field was relaxed to the climatological annual cycle of Levitus et al. (1994) using a relaxation timescale of 50 days. All of the analyses assimilated subsurface temperature measurements from XBTs and the TAO array of moored buoys (McPhaden 1993). To reduce the data management burden for this group of experiments, we used the gridded, monthly SST analyses of Reynolds and Smith (1994) in place of direct measurements of SST.

The first of the experimental analyses, RA5, was produced with our previous analysis system. It has none of the improvements described in section 2. The model has weak vertical mixing and in the assimilation the first-guess error covariance has no zonal stretching of the horizontal scale and no vertical variation in the error variance. For the second analysis, CTL, the model has the strengthened vertical mixing and the first-guess error covariance does have zonal stretching of the horizontal scale, but no vertical variation in the error variance. The last of the analyses, RA6, includes all of the improvements: stronger vertical mixing, zonal stretching of the horizontal covariance scale, and vertical variation in the error variance. A fourth experiment, FSU, is a simulation; the model used is identical to that in CTL and

TABLE 1. Comparison of model analyses.

Analysis	υ_0 ($cm^2\ s^{-1}$)	Horizontal correlation scale	Vertically varying error variance	Period
RA5	5	Isotropic	No	January/1981–June/1995
CTL	50	Anisotropic	No	January/1980–December/1995
RA6	50	Anisotropic	Yes	January/1980–December/1995
FSU	50	No data assimilation		January/1980–December/1995

RA6, but there is no data assimilation. The characteristics of the experiments are summarized in Table 1.

4. Results

In this section the results of RA5 and RA6 are compared to two independent datasets: equatorial currents from moored buoys at 110°W, 140°W, and 165°E and subsurface temperatures at these same sites. All four analyses are compared with independent sea level measurements from the island tide gauge network (Wyrtki 1979).

a. Equatorial currents

Acero-Schertzer et al. (1996) has compared mean surface currents in earlier versions of our analyses with surface drifter data from the TOGA–WOCE (Tropical Ocean and Global Atmosphere–World Ocean Circulation Experiment) surface velocity program (SVP) and found that the mean surface currents in the analyses were too strong in the western equatorial Pacific and too strongly divergent in the eastern equatorial Pacific. The two top panels of Fig. 3 show the average surface currents (at 10-m model depth) for RA5 and RA6 for the period 1981–94. The differences between the two analyses, shown in panel 3, are clear: RA6 is less divergent than RA5 in the eastern equatorial Pacific, and RA6 has weaker westward surface currents than RA5 in the far western equatorial Pacific. As compared to RA5, the average surface currents in RA6 are closer to the average current estimates from surface drifters for 1978–94 shown in Acero-Schertzer et al. (1996). The average meridional gradient of zonal velocity $\overline{u}$ at (0°, 140°W) between May 1990 and June 1991 is 1.4×10^{-6} s^{-1} for RA5 and about half that or 0.77×10^{-6} s^{-1} for RA6. An estimate of $\overline{u}$ from moored buoys at this location for the same 13-month period is 0.75×10^{-6} s^{-1} (Qiao and Weisburg 1997). These comparisons suggest that the RA6 surface currents have improved relative to the RA5 analysis.

Figure 4 compares average zonal velocity profiles from RA5 and RA6 to measurements at three locations on the equator: 110°W, 140°W, and 165°E. The measurements at 110°W and 140°W were made between January 1991 and December 1994 with mechanical current meters; the measurements at 165°E were made between April 1992 and December 1994 by acoustic Doppler current profiler (ADCP). At the eastern equatorial Pacific sites of 110°W and 140°W, the average core depth of the Equatorial Undercurrent is deeper in RA6 than in RA5 and is closer to the observations. The shallow undercurrent core in RA5 is the result of weak vertical mixing and, consequently, less downward transfer of westward surface momentum. At 165°E, the average surface flow in both RA5 and RA6 is westward, while the measured average is close to zero. The undercurrent in RA6 is stronger than in RA5 and above 200 m both are stronger than that measured by the ADCP. The comparison at this site remains a puzzle, the average dynamics in the model analyses appears to be very different than that reflected in the ADCP measurements.

b. Equatorial temperature

Figure 5 compares the depth of the 20°C isotherm for RA5, RA6 and mooring data at three equatorial sites, 110°W, 140°W, and 165°E, between 1992 and 1995. The mooring data for this period were not assimilated and thus are independent of the analyses. The rms differences between the analyses and the moorings are shown in the figure. At both 165°E and 140°W, the rms difference between RA6 and the mooring is less than that for RA5, indicating improvement in the new analysis. At 110°W, the rms difference between RA6 and the mooring is higher than between RA5 and the mooring. The greater rms difference between RA6 and the mooring is largely due to the fact that the average depth of the 20°C isotherm in RA6 is 7.7 m shallower than the mooring estimate. This suggests that RA5 and RA6 actually give different fits to data, while the mean depth of the 20°C isotherm is better in RA5, the variations in the depth of the isotherm are better in RA6. In this sense, the criterion for ''better analysis'' will depend on the purpose for these analyses.

c. Sea level

Measurements of in situ sea surface height variability are available from the tide gauge network. These tide gauge data are not used in the assimilation and are independent of the analyses. Because the sea surface heights are measured relative to an uncertain mean, we compare only monthly anomalies from mean annual cycles. Figure 6 shows the sea surface height anomalies from RA5, RA6, and tide gauge data at four tropical island stations: Yap (9.5°N, 138°E), Truk Moen (7.4°N,

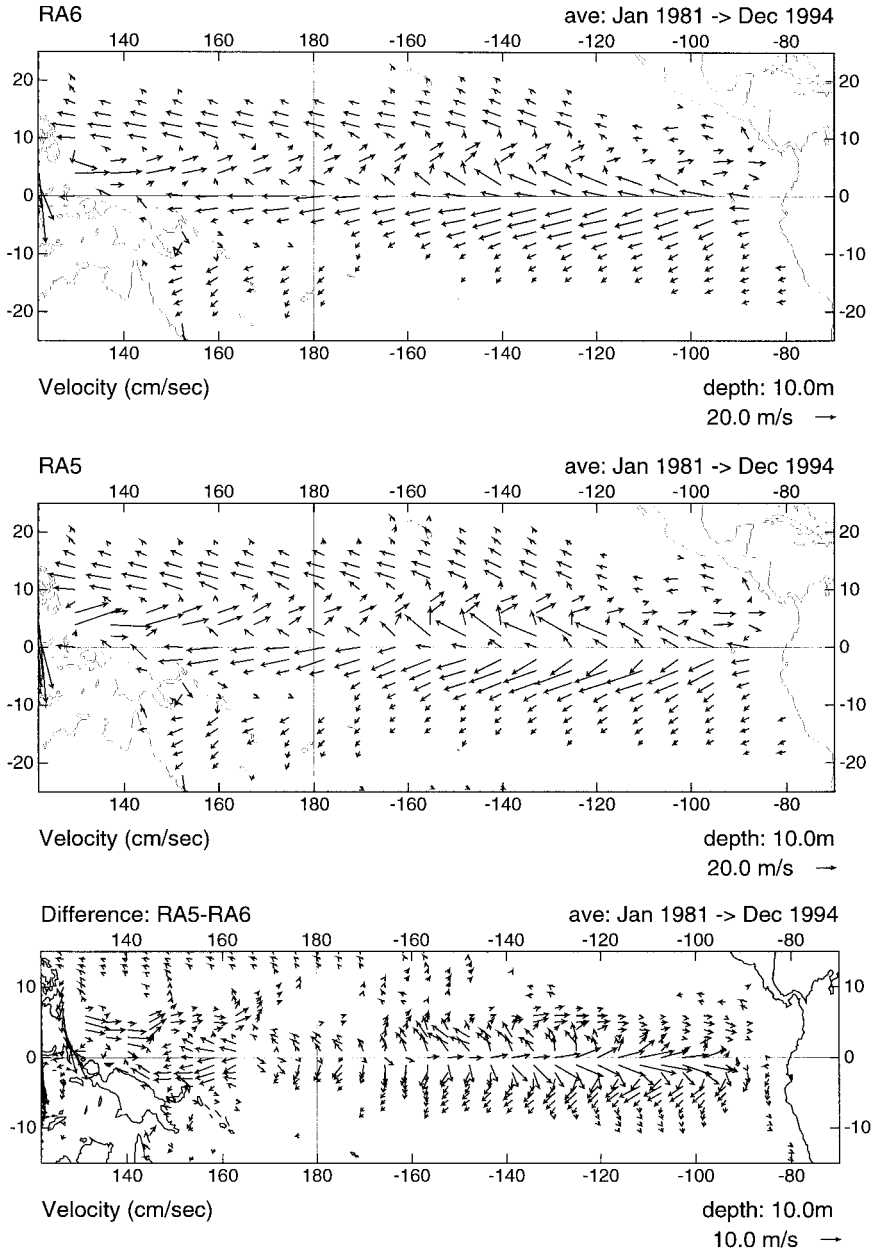

FIG. 3. Mean surface currents (at 10-m model depth) averaged for 1981–94 for RA6 (top) and RA5 (middle) analyses and the difference field (lower). The unit is centimeters per second.

152°E), Funafuti (8.5°S, 179°E), and Honiara (9.4°S, 160°E). The anomalies for each dataset were computed relative to their respective 1981–94 mean annual cycles. Also shown on Fig. 6 are the rms differences between the sea surface height anomalies from four analyses (RA5, RA6, CTL, FSU) and those estimated from the tide gauges. The rms differences for RA6 are consistently the smallest. The rms differences for RA5 are 1–2 cm larger than for RA6. The rms differences for the CTL analysis, which is similar to RA6, but does not include vertical structure in the first-guess error variance used for the assimilation, lie between those for RA5 and RA6. The rms differences for the FSU experiment, which is a simulation and has no data assimilation, are comparable to those for RA5.

A broader comparison of sea surface height anomalies from RA5, CTL, and RA6 with 29 tide gauges within 20° of the equator is shown in Table 2. Two time periods are included: from January 1981 to July 1995 and the more recent period from January 1991 to July 1995 when there was a significant increase in the amount of temperature data available to be assimilated because of the completion of the TAO array. For both periods the rms differences between RA6 and tide gauges are the

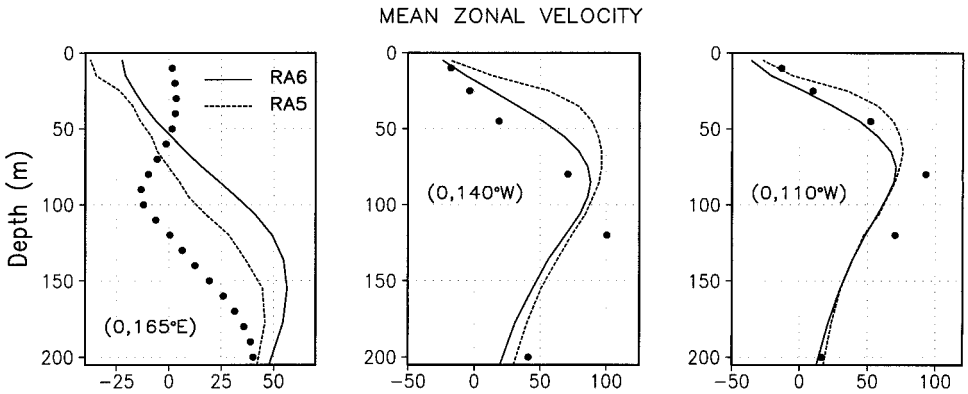

FIG. 4. Mean zonal velocity profile at 110°W, 140°W (averaged for January 1992–December 1994) and at 165°E (averaged for April 1992–December 1994). Solid (dash) lines are from RA6 (RA5) analyses; solid dots are current meter (110°W and 140°W), and ADCP (165°E) observations.

smallest and the addition of the TAO mooring data in the 1990s reduce the rms difference from 4.7 to 3.8 cm. The rms differences for RA5, for both time periods, are about 1 cm larger than those for RA6 and the rms differences for CTL lie between RA5 and RA6.

5. Discussion

In section 4, we compared the model analyses with independent observations of currents, temperature, and sea surface height anomalies. As measured by the comparability of the analyses to the observations, the changes made to the analysis system between RA5 and CTL and between CTL and RA6 are clearly improvements. By briefly comparing the analyses with each other, we can see how these improvements affect their internal structure.

Figure 7 shows zonal sections of temperature from RA5, CTL, and RA6. The sections are for for October 1994, along 8°N. These sections are also typical of other months. Although the large-scale structure is similar in all of the analyses, it is obvious that CTL is smoother than RA5 and RA6 is the smoothest of all. It appears that increasing the zonal scale of the first-guess error covariance function used for the assimilation leads to a smoother analysis (CTL vs RA5) and adding vertical structure to the first-guess error covariance function leads to a still smoother analysis (RA6 vs CTL). As the analyses in this sequence become less noisy they also compare more closely with the observations.

Figure 8 shows equatorial sections of the average daily temperature correction due to data assimilation between January 1991 and December 1995 for the RA6 and CTL analyses (these data were not saved for RA5). Although the contours in both panels are similar, the temperature correction for RA6 has been increased by a factor of 4 for display purposes. Thus, the average daily temperature corrections for CTL were about three to four times larger than those for RA6. By adding vertical structure to the first-guess error covariance function and by our choice of the scaling parameter a_v, which appears in (4), the overall estimate of the first-guess error used in the assimilation is reduced for RA6 as compared to CTL. In other words, in the RA6 analysis the model is given more weight relative to the data than in the CTL analysis. The result is a smoother analysis.

A fundamental problem with our analysis system is that the model, forced only by surface boundary con-

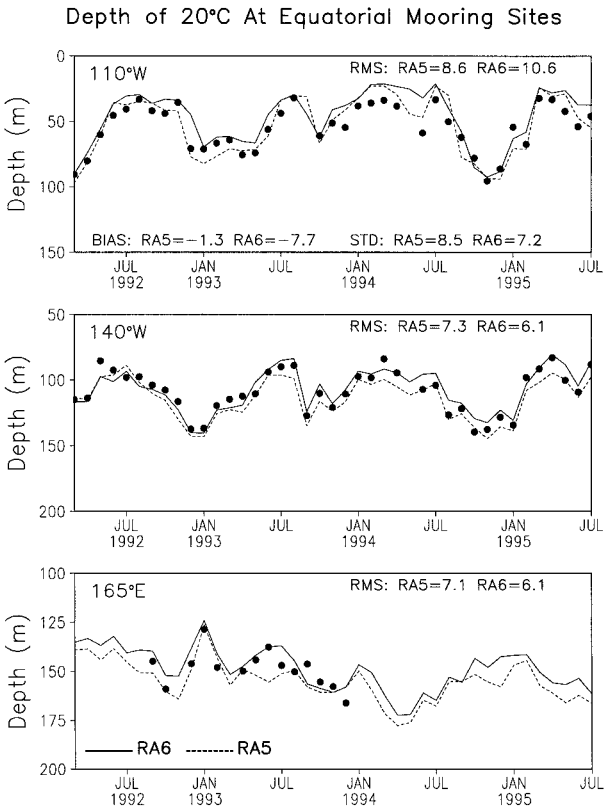

FIG. 5. Observed and analyzed depth of 20°C isotherms at 110°W, 140°W, and 165°E. Solid (dash) curves are from RA6 (RA5) analyses; solid dots are mooring observations.

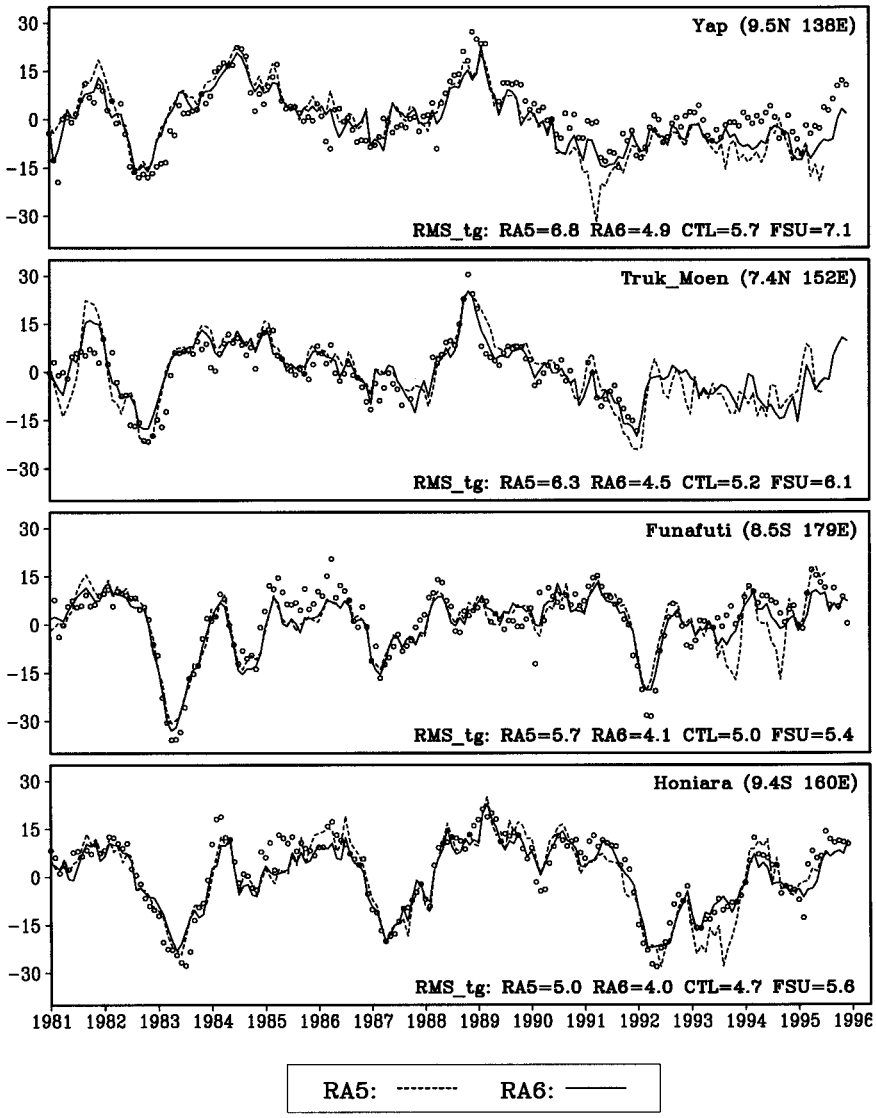

FIG. 6. Monthly mean sea level anomalies at four tide gauge island stations. Solid (dash) lines are analyses from RA6 (RA5), respectively; open circles are tide gauge observations. Anomalies were estimated by removing the respective 1981–94 annual cycle from each dataset.

ditions and assimilating no data, will produce a different mean temperature field than that which is observed (Leetmaa and Ji 1995). The differences can have a large scale and will depend on the averaging period. One of the effects on the analysis system can be seen in Fig. 8. The 5-yr average temperature corrections show persistent negative corrections in the west and positive corrections in the east; the assimilation system uses data to correct the model mean thermocline, pushing it toward the observed mean thermocline by raising it in the west and lowering it in the east. The model responds to these corrections as perturbations to its own mean thermocline and as it adjusts to these perturbations the result is a noisy analysis. Where data is more sparse, for example toward the edges of the TAO array at 8°S and 8°N, it becomes more difficult to sustain the mean correction and the analysis becomes noisier. This is the effect seen in Fig. 7.

TABLE 2. Comparison of model analyses to 29 tropical island tide gauges.

rms differences in anomalous sea surface height (cm)		
Analysis	January 1981–June 1995	January 1991–June 1995
RA5	5.5	4.8
CTL	5.4	4.3
RA6	4.7	3.8

The proper solution to this problem is a better model and forcing by better surface boundary conditions, which will produce a mean temperature that is closer

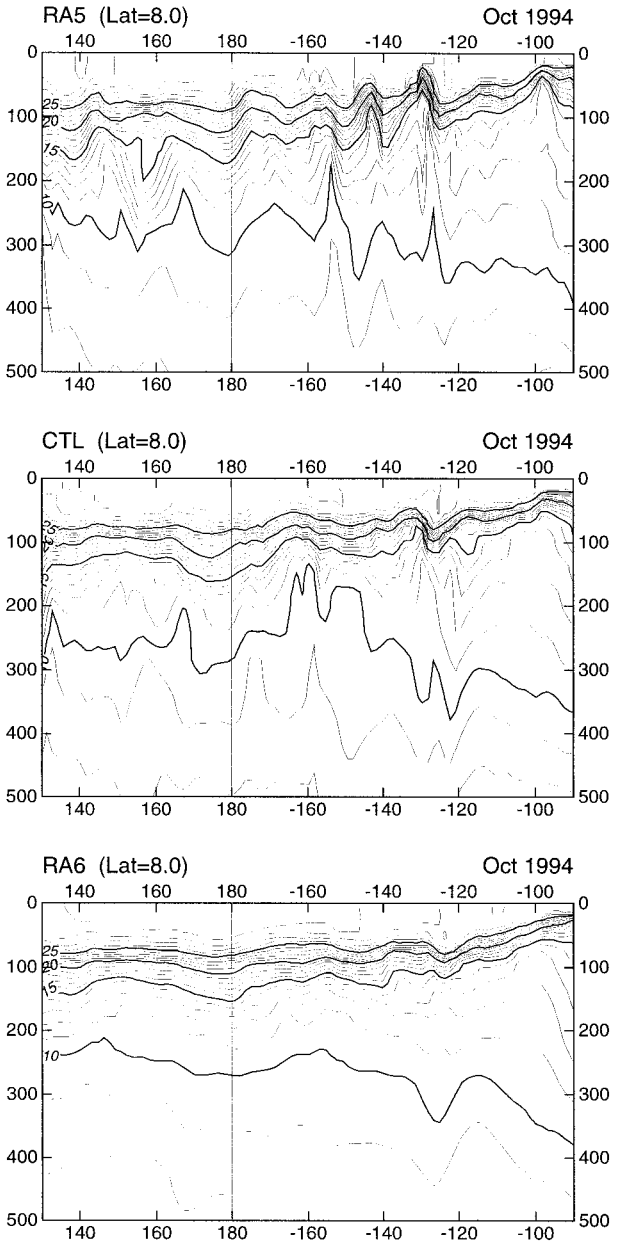

FIG. 7. Vertical cross section of temperature along 8°N for October 1994. Shown from top to bottom are RA5, CTL, and RA6 analyses, respectively. Contour intervals are 1°C.

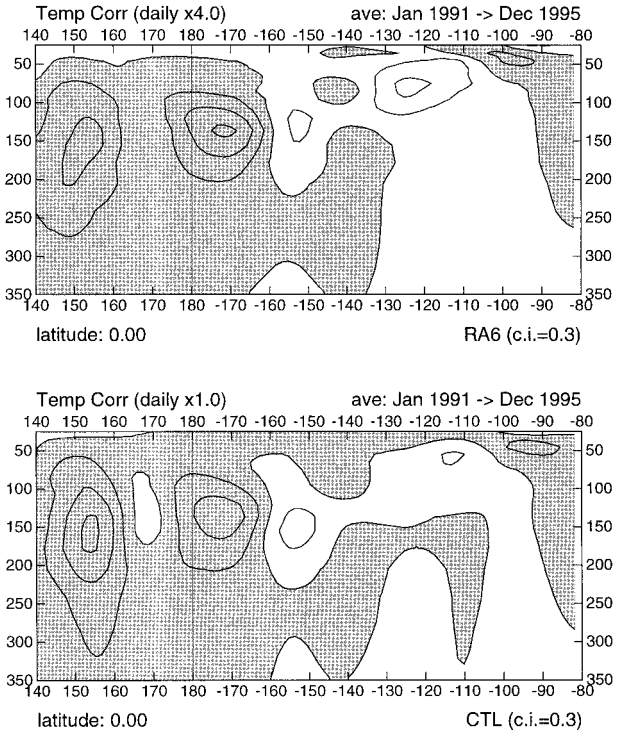

FIG. 8. Daily mean temperature correction due to data assimilation along the equator averaged for 1991–95. Shown for the RA6 analysis (the upper panel) are four times the actual daily mean temperature correction; shown for the CTL analysis (the lower panel) are the actual daily mean temperature correction. Contour intervals are 0.3°C.

to what is observed. In the absence of that, RA6 manages a balance between model and data that produces a relatively noise-free analysis by giving more weight to the model, that is, using stronger dynamical constraint. These analyses compare better with the large-scale variability in observations (on timescales of a month or more) than do older analyses which give more weight to the observations. However, the strong dynamical constraint strategy for RA6 may lead to less effective correction of the mean model-forcing system error, as evidenced in the comparison of the mean depth of the 20°C isotherm at 110°W on the equator (Fig. 5). The effect of these analyses when they are used to initialize ENSO forecasts is the subject of Part II of this paper.

6. Summary

In this paper, we describe a new version of the NCEP ocean analysis system that incorporates a number of modifications to the system described in Ji et al. (1995). Three sets of Pacific Ocean analyses, RA5, CTL, and RA6, are described and compared with independent observations of equatorial temperatures and currents from moored buoys and tropical Pacific sea level variations from tide gauges. The comparisons showed that the new analysis system produced more accurate ocean analyses, when compared to observations, than the original system.

Much of the improvement is due to a new representation of the first-guess error covariance used in the data assimilation. The new error covariance concentrates the temperature corrections in the thermocline and represents an overall reduction in the magnitude of the first-guess error. The effect is to increase the weight for the model relative to the data in the assimilation, which implies stronger dynamical constraint. The result is a

less noisy analysis that compares better with observations.

At NCEP, the primary purpose of the ocean data assimilation system is to produce initial ocean conditions for a coupled ocean–atmosphere model for forecasting ENSO. In Part II of this paper, we show that the new data assimilation scheme contributes significantly to improving ENSO forecast skill.

Acknowledgments. The authors wish to express our gratitude to Dr. David Halpern (NASA/JPL) and Dr. Deng-Hua Wu (NCEP/GSC) for their help on analyzing currents and temperature data from the equatorial moorings. TAO and mooring data at 110°W, 140°W, and 165°E were obtained from NOAA/PMEL. Tide gauge data were obtained from the TOGA sea level center at the University of Hawaii. Support for this research is provided by NOAA's Office of Global Program through the Climate and Global Change Program.

REFERENCES

Acero-Schertzer, C. E., D. V. Hansen, and M. S. Swenson, 1997: Evaluation and diagnosis of surface currents in the NCEP ocean analyses. *J. Geophys. Res.,* **102,** 21 037–21 048.

Bryan, K., 1969: A numerical method for the study of the World Ocean. *J. Comput. Phys.,* **4,** 347–376.

Cane, M. A., S. E. Zebiak, and S. C. Dolan, 1986: Experimental forecasts of El Nino. *Nature,* **321,** 827–832.

Chen, D., S. E. Zebiak, A. J. Busalacchi, and M. A. Cane, 1995: An improved procedure for El Nino forecasting. *Science,* **269,** 1699–1702.

Cox, M. D., 1984: A primitive, 3-dimensional model of the ocean. GFDL Ocean Group Tech. Rep. 1, Geophysical Fluid Dynamics Laboratory/NOAA, Princeton University, 143 pp. [Available from Geophysical Fluid Dynamics Laboratory/NOAA, Princeton University, Princeton, NJ, 08540.]

Derber, J. D., and A. Rosati, 1989: A global oceanic data assimilation system. *J. Phys. Oceanogr.,* **19,** 1333–1347.

Hellerman, S., and M. Rosenstein, 1983: Normal monthly wind stress over the world ocean with error estimates. *J. Phys. Oceanogr.,* **13,** 1093–1104.

Ji, M., A. Kumar, and A. Leetmaa, 1994: An experimental coupled forecast system at the national meteorological center: Some early results. *Tellus,* **46A,** 398–418.

——, A. Leetmaa, and J. Derber, 1995: An ocean analysis system for seasonal to interannual climate studies. *Mon. Wea. Rev.,* **123,** 460–481.

——, D. W. Behringer, and A. Leetmaa, 1998: An improved coupled model for ENSO prediction and implications for ocean initialization. Part II: The coupled model. *Mon. Wea. Rev.,* **126,** 1022–1034.

Kirtman, B. P., J. Shukla, B. Huang, Z. Zhu, and E. K. Schneider, 1997: Multiseasonal predictions with a coupled tropical ocean–global atmosphere system. *Mon. Wea. Rev.,* **125,** 789–808.

Kleeman, R., 1993: On the dependence of hindcast skill in a coupled ocean–atmosphere model on ocean thermodynamics. *J. Climate,* **6,** 2012–2033.

——, A. M. Moore, and N. R. Smith, 1995: Assimilation of subsurface thermal data into a simple ocean model for the initialization of an intermediate tropical coupled ocean–atmosphere forecast model. *Mon. Wea. Rev.,* **123,** 3103–3113.

Latif, M., A. Sterl, E. Maier-Reimer, and M. M. Junge, 1993: Structure and predictability of the El Nino/Southern Oscillation phenomenon in a coupled ocean–atmosphere general circulation model. *J. Climate,* **6,** 700–708.

Leetmaa, A., and M. Ji, 1995: Ocean data assimilation as a component of a climate forecast system. *Modern Approaches to Data Assimilation in Ocean Modeling,* P. Malanotte-Rizzoli, Ed., Elsevier, 271–293.

Levitus, S., R. Burgett, and T. P. Boyer, 1994: *World Ocean Atlas 1994, Vol. 3: Salinity.* NOAA Atlas NESDIS 3, 99 pp.

McPhaden, M. J., 1993: TOGA-TAO and the 1991–93 El Nino–Southern Oscillation event. *Oceanogr.,* **6,** 36–44.

Oberhuber, J. M., 1988: An atlas based on the ''COAS'' data set: The budgets of heat, buoyancy and turbulent kinetic energy at the surface of the global ocean. Rep. 15, Max-Planck-Institut fur Meteorologie, 20 pp.

Pacanowski, R., and S. G. H. Philander, 1981: Parameterization of vertical mixing in numerical models of tropical oceans. *J. Phys. Oceanogr.,* **11,** 1443–1451.

Philander, S. G. H., W. J. Hurlin, and A. D. Seigel, 1987: A model of the seasonal cycle in the tropical Pacific Ocean. *J. Phys. Oceanogr.,* **17,** 1986–2002.

Qiao, L., and R. H. Weisberg, 1997: The zonal momentum balance of the Equatorial Undercurrent in the central Pacific. *J. Phys. Oceanogr.,* **27,** 1094–1119.

Reynolds, R. W., and T. M. Smith, 1994: Improved global sea surface temperature analysis using optimum interpolation. *J. Climate,* **7,** 929–948.

Rosati, A., K. Miyakoda, and R. Gudgel, 1997: The impact of ocean initial conditions on ENSO forecasting with a coupled model. *Mon. Wea. Rev.,* **125,** 754–772.

Stricherz, J., J. J. O'Brien, and D. M. Legler, 1992: *Atlas of Florida State University Tropical Pacific Winds for TOGA 1966–1985*. The Florida State University, 275 pp.

Wyrtki, K., 1979: Sea level variations: Monitoring the breath of the Pacific. *Eos, Trans. Amer. Geophys. Union,* **60,** 25–27.

Zebiak, S. E., and M. A. Cane, 1987: A model El Nino–Southern Oscillation. *Mon. Wea. Rev.,* **115,** 2262–2278.